Journal of Micromechanics and Microengineering

PAPER

# A mass manufacturable thermoplastic based microfluidic droplet generator on cyclic olefin copolymer



IOP Publishing Journal of Micromechanics and Microengineering
J. Micromech. Microeng. **29** (2019) 055009 (9pp) https://doi.org/10.1088/1361-6439/ab0e60

# A mass manufacturable thermoplastic based microfluidic droplet generator on cyclic olefin copolymer

**Sthitodhi Ghosh[1], Gopakumar Kamalakshakurup[2], Abraham P Lee[2] and Chong H Ahn[1]**

[1] Department of Electrical Engineering and Computer Science, Microsystems and BioMEMS Laboratory, University of Cincinnati, Cincinnati, OH, United States of America
[2] Department of Biomedical Eng., CADMIM—NSF I/UCRC Center for Advanced Design and Manufacturing of Integrated Microfluidics, UC, Irvine, CA, United States of America

E-mail: ahnch@ucmail.uc.edu

Received 20 February 2019
Accepted for publication 8 March 2019
Published 10 April 2019

**Abstract**

The rapid progress of droplet microfluidics and its wide range of applications have created a high demand for the mass fabrication of low-cost, high throughput droplet generator chips aiding both biomedical research and commercial usage. Existing polymer or glass based droplet generators have failed to successfully meet this demand which generates the need for the development of an alternate prototyping technique.This work reports the design, fabrication and characterization of a mass manufacturable thermoplastic based microfluidic droplet generator on cyclic olefin copolymer (COC). COC chips with feature size as low as 20 $\mu$m have been efficiently fabricated using injection molding technology leading to a high production of inexpensive droplet generators. The novelty of this work lies in reoptimising surface treatment and solvent bonding methods to produce closed COC microchannels with sufficiently hydrophobic (contact angle of 120°) surfaces. These COC based droplet generators were shown to generate stable monodisperse droplets at a rate of 1300 droplets/second in the dripping regime. These new mass manufacturable, disposable and cheap COC droplet generators can be custom designed to cater to the rapidly increasing biomedical and clinical applications of droplet microfluidics.

Keywords: droplet generator, cyclic olefin copolymer (COC), injection molding

(Some figures may appear in colour only in the online journal)

## 1. Introduction

The advancement of microfluidic technology in the early century has led to the revolution in the sensing and detection of chemical and biological samples [1]. Over the last few decades, the presence of microfluidics has steadily increased in applications such as emulsification, biomedical diagnostics and drug screening [2]. The use of considerably less sample volumes or reagents, a shorter diagnostic time due to the high surface-to-volume ratio, and significantly inexpensive technology are some of the unique advantages of microfluidics over traditional techniques. The samples and reagents in nl to $\mu$l volumes are analysed in lab-on-a-chip devices using either single phase [3] or multiphase (droplets) methodologies [2, 4].

Notably, droplet microfluidics is an emerging platform that has already made significant impact in the life science industry in less than a decade. Droplet serves as an isolated reaction containers of ultra-low sample volumes, and the possibility of liquid handling unit operations at high throughput makes it a powerful platform for applications including single cell sequencing [5], drug discovery [6], directed evolution [7], and various genomic and proteomic assays [8]. In addition, rapidly evolving microfluidic technologies have enabled droplets to be used as liquid reaction containers for screening

 

protein crystallization conditions [9–11], as micro-templates for assisting self-assembly of materials [12–15], and as components for micro-electrical actuation [16]. Droplet based polymerase chain reaction (PCR) [17–19] and DNA analysis [20] have also been successfully demonstrated using droplet-based microfluidic system.

Although droplet microfluidics is a commerically viable technology with recent successes [21], one of the major challenges is the material choice for the fabrication of the microfluidic devices [22]. Polydimethylsiloxane (PDMS) is one of the major materials used in polymer microfluidics due to its material elasticity, gas permittivity and other unique advantages. Ease of fabrication, superior elastomeric properties, high optical transmissivity, excellent biocompatibility and an inherent hydrophobic surface makes PDMS an ideal material for most droplet based microfluidic devices that have been reported [17, 19, 23–25]. However, PDMS casting and curing process is time consuming (0.5–2 h) which limits high-volume production of PDMS microfluidic devices. PDMS is also associated with problems including swelling and deformation on exposure to organic solvents, low acid/base resistivity, autofluorescent, leaching and evaporation, which makes it inappropriate for commercialization [26]. As an alternative, glass is used as a material for microfluidic devices [27]; however, the fabrication process is tedious and the cost per chip is high. Therefore, successful commercialization of the droplet based devices strongly demands the need for a cheap, mass manufacturable material and fabrication method for the development of a mass producible and robust polymer chip for the droplet generators.

Thermoplastics are rigid polymer materials with good mechanical stability, a low water-absorption percentage, and organic-solvent and acid/base resistivity, which are critical factors in many bioanalytical microfluidic applications [28]. The thermoplastic cyclic olefin copolymer (COC) has been reported to be ideal for PCR and other immunodiagnostic applications [29–31]. Thus COC based droplet generators have the potential to accelerate the development of low cost, disposable droplet PCR and other diagnostic platforms. However, COC by nature is not hydrophobic and hence does not support the formation of water-in-oil droplets. The COC surface can be treated to obtain the desired hydrophobicity; however the hydrophobic surface leads to poor fusion bonding and thus hinders the development of a closed channel microfluidic device. A reported solvent bonding method [32] was carefully revisited in this work and reoptimised to bond hydrophobic surfaces of COC to form closed hydrophobic microchannels facilitating reliable droplet generation. The injection molding method as reported by Ahn *et al* [33] was reoptimised in this work to fabricate a Nickel micromold with a minimum feature size of 20 $\mu$m, which was used to produce polymer replicates by injection molding. Although most of the microfabrication steps have been previously reported, the novelty of this work lies in combining the methods to develop a robust droplet generator. This paper for the first time reports the development of a flow focusing microfluidic droplet generator on the COC substrate to ensure mass production, increased reliability and lower cost.

## 2. Principles

One of the capabilities of droplet microfluidics is that it can perform numerous unit operations, of which the generation of monodisperse droplet libraries is of the utmost importance. Over the years, a variety of techniques have been developed for droplet generation [2]. However, the most commonly used are the T-junction and flow focusing channel geometry. In flow focusing configuration, both the dispersed phase and the continuous phase are forced to pass through a narrow orifice in the microfluidic channel [34–36]. Symmetric shearing by the continuous phase on the dispersed phase enables more controlled and stable generation of droplets. An extension of flow-focusing is shear-focusing, which aims to create a singular point of highest shear. This ensures that the break-off of droplets from the fluid stream occurs consistently at that point thus forming uniform droplets [35]. The expanding nozzle design as reported by Lee *et al* [35] generates a velocity gradient in the flow direction that allows the droplet to break at the location of maximum shear stress and pressure point, which is at the orifice. A similar concept was used to design the droplet generators in this work to compare the functionality of COC based droplet generators to that of the reported PDMS devices.

The overall design of the intended droplet generator is shown in figure 1(a) which consists of two inlets (e.g. one for oil and the other for the aqueous phase), a pressure reservoir for stabilizing the oil and aqueous phase, an expanding nozzle to focus and dissipate the force of the flow and an outlet for the collection of the droplets. The schematic of the basic concept of droplet generation at the orifice is shown in figure 1(b) where oil and water phases are forced to pass through a narrow orifice. As shown in figure 1(c) [35], in the expanding nozzle design, fluid velocity increases before entering the nozzle. The fluid velocity becomes maximum at the orifice and then gradually decreases as it exits the orifice. As a result, a high velocity gradient around the orifice of the nozzle is created. The nozzle design is shown in figure 1(d). The channels have a uniform depth of 50 $\mu$m and the nozzle has an orifice width of 20 $\mu$m.

Droplet generators with different orifice sizes and a droplet splitter design for high throughput generation of droplets were incorporated in a single design as shown in figure 2(a). Smaller nozzle dimension leads to stabler droplet generation and hence orifices with different width sizes (10 $\mu$m, 20 $\mu$m and 40 $\mu$m) were designed. However, the devices with 10 $\mu$m orifice width often suffered structural damage during the SU8 removal process of mold fabrication. The droplet generators with 20 $\mu$m orifice width were successfully and reliably fabricated and has been reported here. The droplet splitter with some modifications can be used for droplet PCR applications [37]. The droplet generation is demonstrated in squeezing, dripping, and jetting regimes including the droplet production rates.

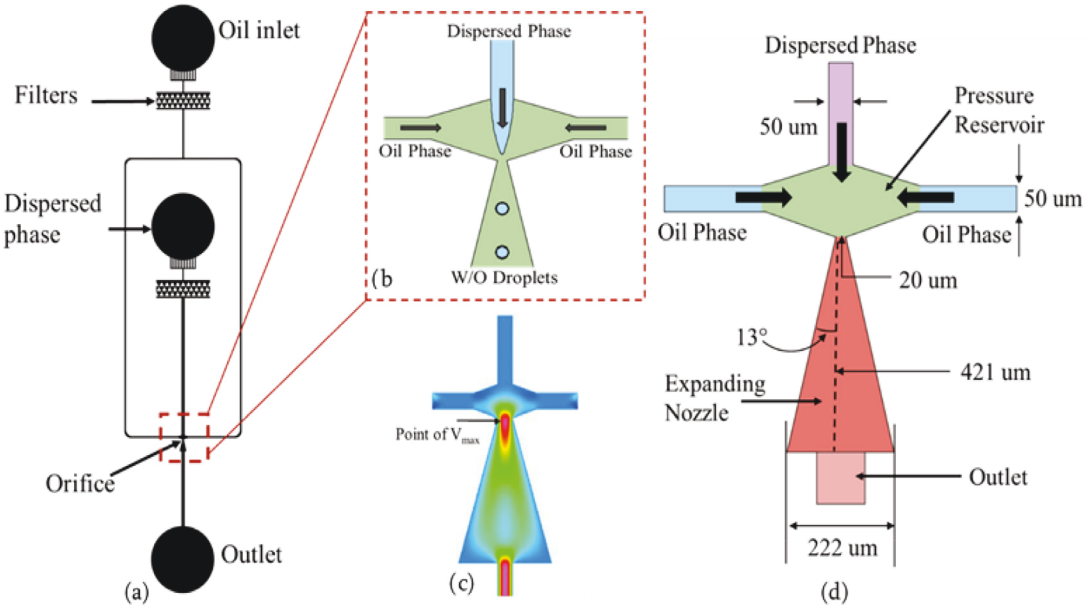


**Figure 1.** (a) Design of the droplet generator with its various parts. (b) Schematic of droplet generation. (c) CFDRC simulation of velocity distributions in orifice connected to an expansion nozzle. This design allows the max velocity to occur at the orifice (reprinted from [35], Copyright 2006, with permission from Elsevier). (d) Schematic of the droplet generation channel geometry. The water phase enters from the middle channel and is sheared by two oil streams at the orifice of the expanding nozzle. The depth of channel is 50 $\mu$m.

## 3. Microfabrication

Successful utilization and customisation of an established replication technology to develop a mass producible, cheap and robust droplet generator is the focus of this paper. COC (Topas 5013S-04) has been used as the substrate material for the polymer lab-on-a-chip because of its high resistance towards polar solvents, very high flow rates during injection molding and high biological compatibility [38]. COC exhibits optical transparency over a wide range including the UV spectrum which makes it ideal for biochemical analysis and bio-optical application [39].

The fabrication process consists of fabricating a high precision metallic micro-mold insert and polymer replication using injection molding. The UV LIGA-based plastic micromachining process consists of four main steps: photolithography, electroplating for mold master fabrication, plastic chip fabrication using the metallic mold and finally bonding, as shown in figure 2(b) [40].

### *3.1. Development of insertable disk-mold*

Among the several mass manufacturable methods of polymer lab-on-a-chips, injection molding technology has been considered as one of the most appropriate approaches [41]. The reported disk-mold insert technology [33, 42] can lead to fast and reliable fabrication of custom designed micromolds for injection molding. Microchannels or micro patterns were fabricated on a thick nickel disk using thick photolithography and the desired microstructures were created by controlled electroplating. The patterned nickel disk was then inserted in injection molding block as a master injection mold. Nickel (Ni) disks of 1.6 mm thickness in 100 $\times$ 100 $mm^2$ square shape (Goodfellow Corporation, PA, USA) were cut into circular disks of 3-inch diameter. The 3-inch nickel disks were lapped and polished to eliminate the surface roughness. SU8-2075 (MicroChem Corporation, USA) was used as the template for electroplating. Photolithography with SU8 was optimized for the microfabrication of structures with a uniform height of 50 $\mu$m and a minimum width of 20 $\mu$m. Vertical side walls with exposed Ni surfaces were successfully achieved to facilitate the next electroplating process.

The established electroplating procedure as reported by Ahn *et al* [43] minimized the non-uniformities of electroplating. Electroplating was carried in a bath of Nickel-Sulfamate with the patterned disk as the cathode and pure nickel foil as the anode. The temperature and pH of the solution was maintained at 55 °C and 4.0 respectively. Post-electroplating, the nickel disk was subjected to a polish to remove the over-plated nickel and to obtain a smooth surface. High quality injection molding requires the surfaces of the micro disk-mold to have a surface roughness of around 10 nm. The surface of electroplated Ni was polished gently using cerium oxide solution and colloidal Silica solution to give the mold a mirror finish with desired surface roughness.

Post electroplating, the SU8 layer was removed from the disk in SU8 Remover solution (MicroChem Corporation) heated to 70 °C. However, this resist removal process was not enough to remove the SU8 residues trapped inside minute crevices. It was especially difficult to remove SU8 stuck inside the micro-triangular grooves designed for filtering. These residues cause height-nonuniformity in the replicated chips and cause fouling and leakage. Hence, the resist removal process was followed by a dry etching method to obtain a clean Ni mold without SU8 residue as shown in figure 2(c). The dry etching was performed in Technics™ 85 Reactive Ion Etcher

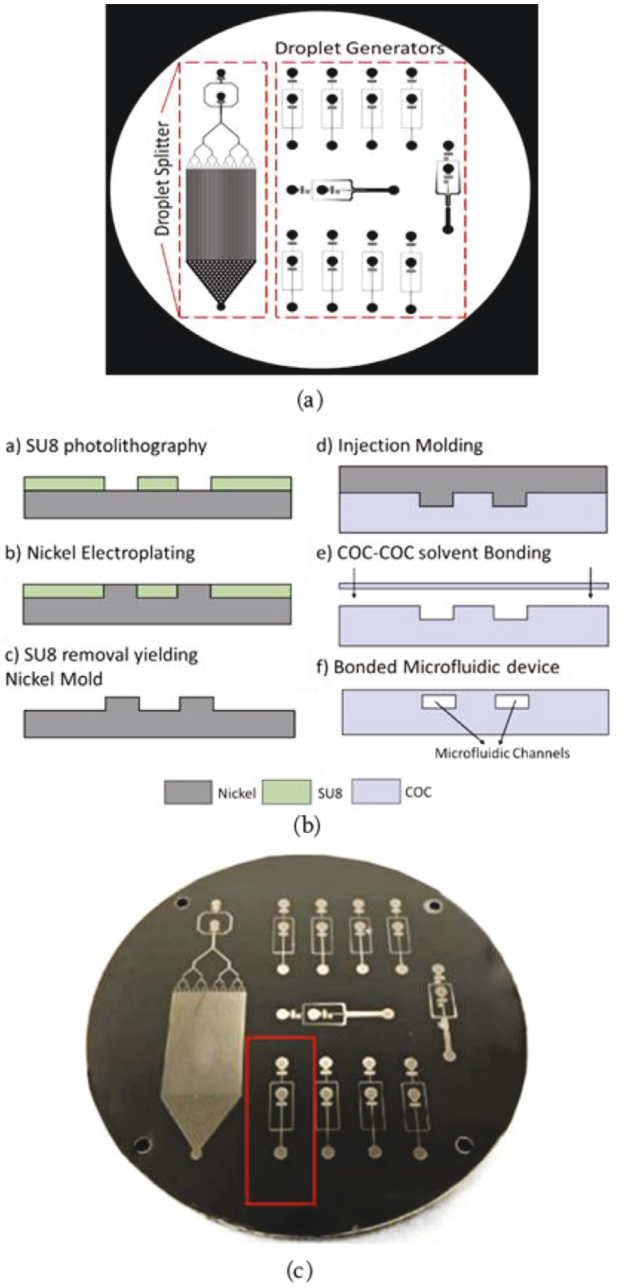


**Figure 2.** (a) The chrome-on-glass photomask used for photolithography. (b) Schematic illustration of the microfabrication steps. (c) Fabricated nickel master mold with the droplet generator marked in red.

using a mixture of $O_2$ and $CF_4$ plasma. The ratio of the $CF_4$ flow rate to $O_2$ flow rate was adjusted to be 1:10. The disk was plasma treated at 100 watts thrice for 5 min with intermittent cooling breaks. The magnified image of the filter area before and after plasma treatment is shown in figure 3(a).

### *3.2. Injection molding with insertable disk-mold*

Injection molding was carried out in a BOY 22A Procan CT (BOY, USA) injection molding machine with the developed nickel disk-mold. As per the processing datasheet of Topas 5013S-04, the injection molding parameters were optimized

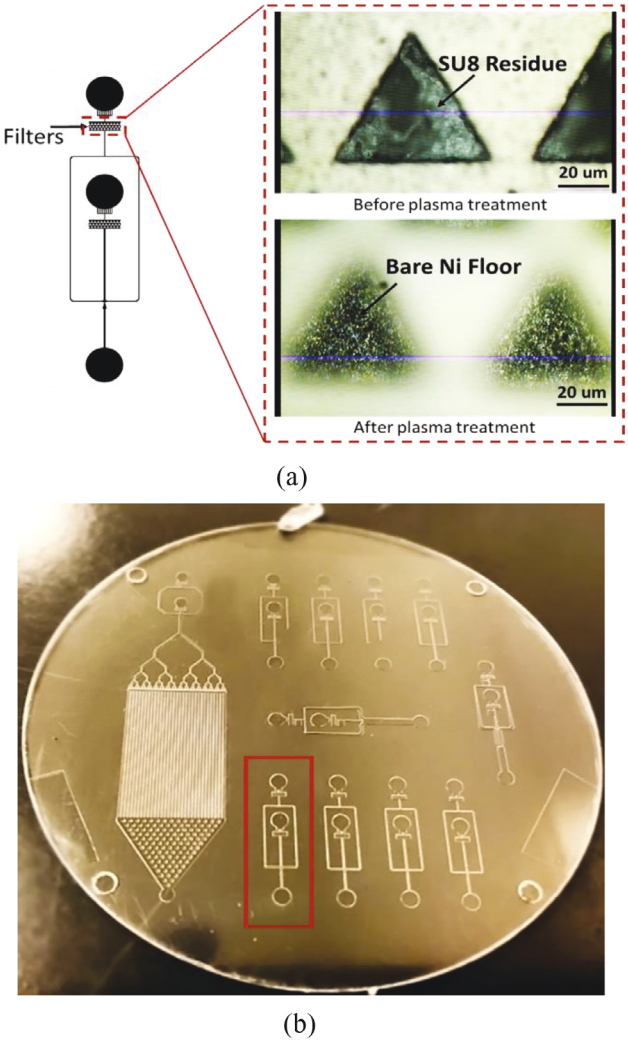


**Figure 3.** (a) Magnified image of the filter area before and after performing plasma based dry etching (b) injection molded COC wafer with the droplet generator marked in red.

**Table 1.** Injection molding properties.

| | |
|---|---|
| Nozzle temperature | 565 °F |
| Mold temperature | 480 °F |
| Speed of injection | 85 mm $s^{-1}$ |
| Back pressure | 2000 psi |
| Cooling time | 15 s |

and is shown in table 1. The process cycle was automated and cycle time was optimized to 32 s thus ensuring even lower injection molding cost and increasing the throughput of the process.

Although the fabrication of the metal mold is more complicated and extensive as compared to the Silicon mold fabricated for PDMS based casting, the advantages are enormous. In general, fabrication of a single PDMS chip from a mastermold takes around 2 h including degassing, casting and curing whereas the COC chips can be fabricated in 32 s as mentioned earlier. This implies that this technology can offer a significantly high volume of production. Moreover, the cost of each produced COC chip is also significantly less than the

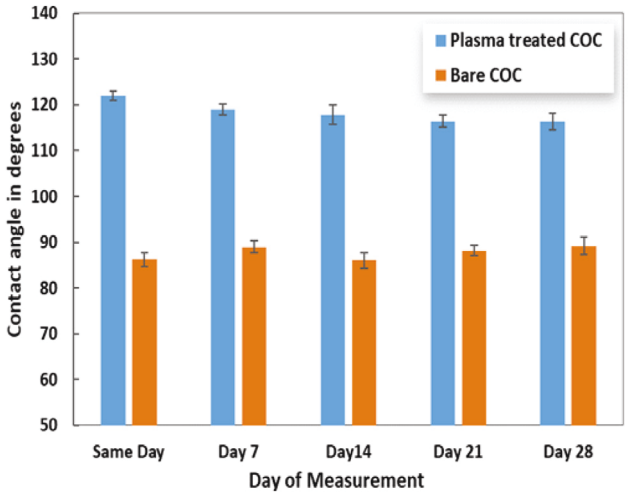


**Figure 4.** Variation of contact angle as a function of time (in days) in plasma treated and bare COC surfaces.

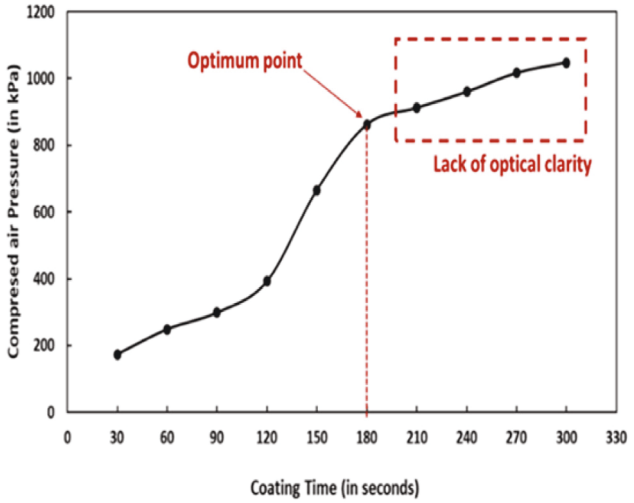


**Figure 5.** Burst pressure test showing the variation of maximum air pressure that the bonding can withstand with the solvent coating time.

cost of each PDMS chip produced. With the increase in the volume of production, even considering the material scraps associated with each injection and allowing for chips rejected on the basis of cleanliness,opacity and quality of ejection, the price of each COC chip can be shown to be extremely less (in the order of a few tens of cents). This makes the cost of good (COG) of each thermoplastic droplet generator much less than that of PDMS or glass based devices. However, implementing a number of identical designs on a single chip and the automated plasticizing process reduced the manufacturing scrap rate. The automated injection molding process also enhanced the reproducibility of the manufactured devices. With a single nickel disk-mold, hundreds of reproducible droplet generator chips were thus fabricated. With the implementation of rapid injection molding process, highly reproducible microstructures were developed on the 3-inch COC wafers as shown in figure 3(b).

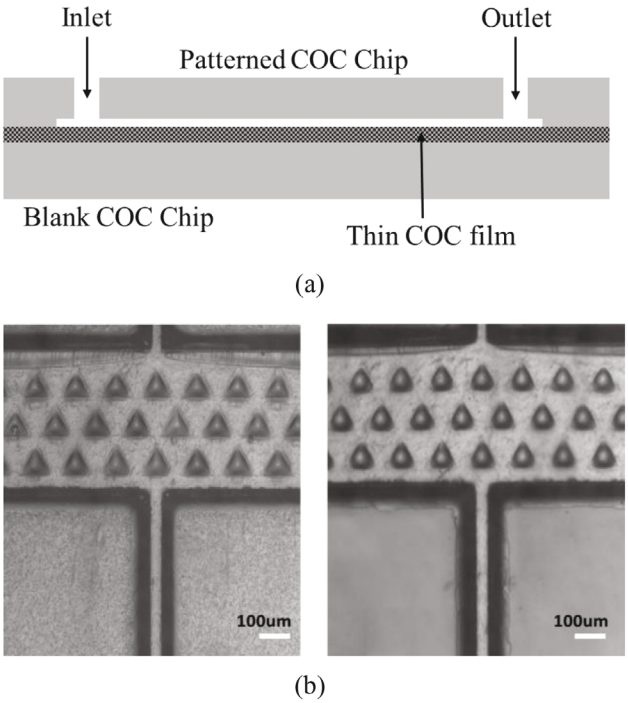


**Figure 6.** Solvent bonding: (a) schematic of the solvent bonding process where the thin film is sandwiched between two COC chips. (b) Injection molded COC microstructures before (left) and after (right) bonding of a thin lid. Microstructures were not deformed by solvent bonding.

### *3.3. Solvent bonding*

Although the size of the orifice of the T-junction or flow-focusing nozzle strongly influences the size of droplets formed, other factors such as the viscosity of the immiscible phases, use of surfactants, and hydrophilicity or hydrophobicity of the channel surface can also be used to augment the size ranges of droplets and particles formed [2]. Surface properties of the microfluidic channels is critical for the generation of stable monodisperse water-in-oil (W/O) droplets. To prevent the discrete phase from adhering to the channel walls, W/O droplets are formed in hydrophobic channels.

The native surface contact angle of an injection molded COC wafer is around 86° with water and hence was found to be not ideal for W/O droplet generation. It has been reported that COC surfaces treated with a mixture of $CF_4$ and $O_2$ plasma gave a higher contact angle, more hydrophobic, as compared to the surfaces treated separately with either of them [44]. In this work, the injection molded patterned wafers were exposed to a mixture of $CF_4$ and $O_2$ plasma in a reactive ion etching machine. The power and time were optimized (150 W for 120 s) to obtain a contact angle of approximately 120°. This behavior can be explained only with a surface chemical change where the $CF_4$ attaches to the surface giving a hydrophobic nature [45].

The wettability of the plasma treated surfaces of COC was characterized in ambient air at room temperature using a contact angle analyzer and is based on the sessile drop method

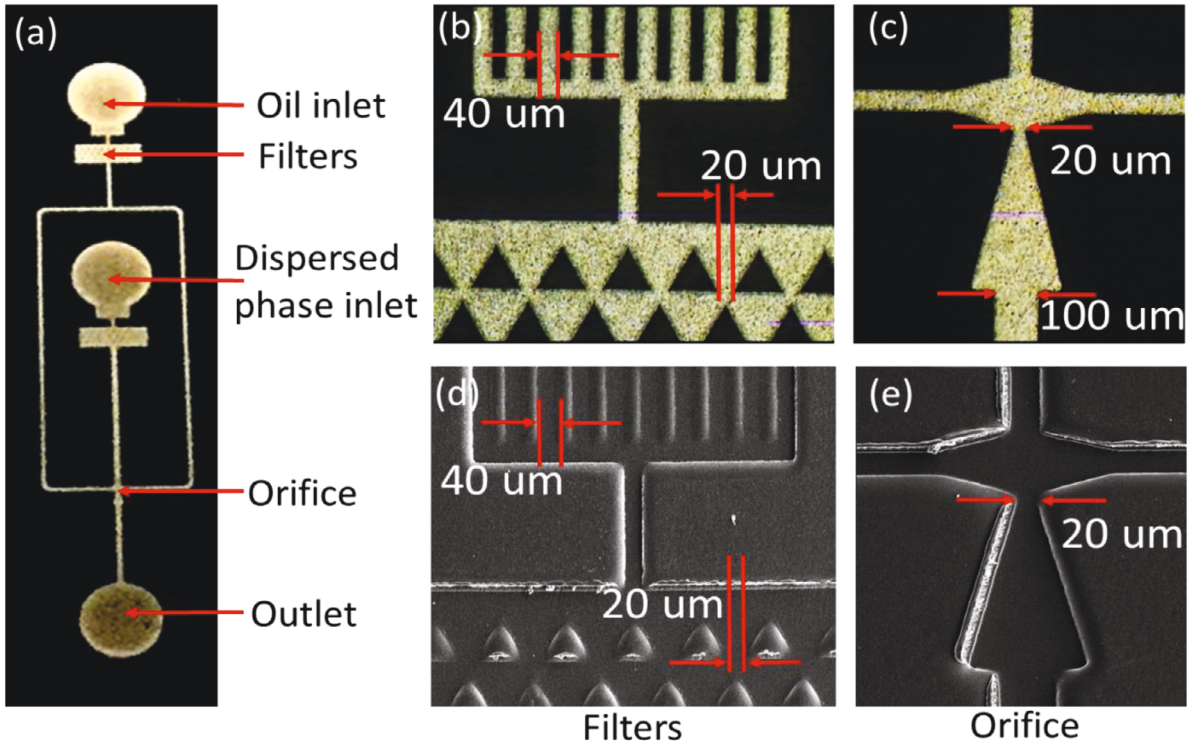


**Figure 7.** Nickel mold: (a) nickel mold of a single device with its various parts. (b) and (c) Magnified images of the filters and the orifice of the mold structure with feature dimensions.(d) and (e) SEM images of the filters and orifice on the COC chip.

that is a simple, but very powerful method for measuring the changes of surfaces at the monolayer level. 2 $\mu$l of DI water was applied on the sample surfaces using a micropipette. The mean contact angles with high purity DI water were determined by averaging values measured at five different points on the sample surface. After plasma treatment, the wafers were stored at room temperature and the contact angle was measured over weeks. Since this surface treatment lowers the surface free energy (more hydrophobic), the contact angle remains stable for days, shown in figure 4.

Although thermal fusion bonding has been reported to be the most reliable method of bonding COC surfaces, the bond strength of thermal fusion bonding greatly depends on the surface condition of the plastic. More hydrophobic the surface is, the bond strength decreases significantly [33]. Considering the fairly hydrophobic surface of the plasma-treated COC, it was impossible to achieve the bonding strength desirable for the high-pressure droplet generation. Thus, a new bonding technique was envisaged for the droplet generator chip.

COC dissolves preferably in non-polar organic solvents such as hydrocarbons, while it is resistant to polar organic solvents like acetone [46]. A cyclohexane based solvent bonding method was reported [32], which showed that dilution of cyclohexane in acetone (35% volume cyclohexane in acetone) prevents the excessive adsorption of solvent by COC thus leading to a bubble free strong solvent bonding which can withstand up to 744 kPa of pressure. This concept was explored and the process reoptimised to bond the hydrophobic COC surface. Topas 8007-S4 COC films of 110 $\mu$m thickness were used for the bonding purpose.

Since the ATR (attenuated total reflectance) spectrum of a $CF_4 + O_2$ plasma treated COC surface shows a strong C–F peak and a C=O peak instead of a strong $CH_2$ peak and a small C–H peak as shown in native COC [45], the nature of penetration of the solvent in the hydrophobic COC surface will be different. This necessitated an optimisation of the solvent bonding process.The thin COC film was cleaned in 2-propanol and was dried with Nitrogen. Two filter papers (Carl Schleicher and Schüll no. 589/3) were soaked with the solvent (a mixture of cyclohexane and acetone) and in the 'coating' step, the COC lid was placed in between the soaked papers. The time of the solvent treatment was optimised to sustain the optical clarity of the untreated COC wafers and to

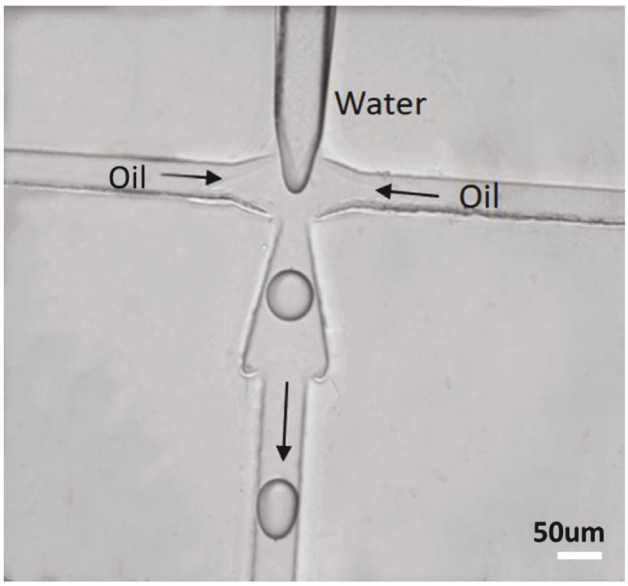


**Figure 8.** Generation of stable monodisperse droplets at the orifice.

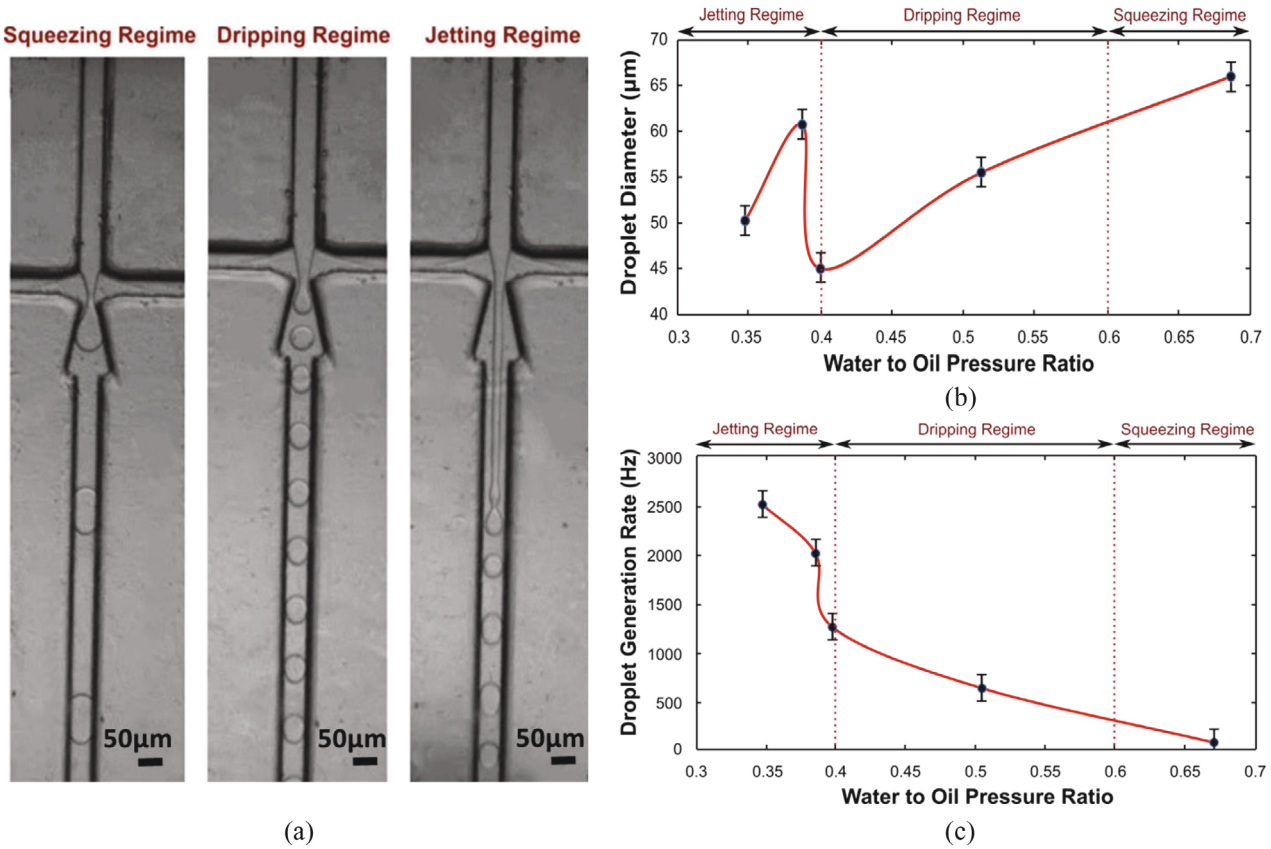


**Figure 9.** (a) Droplet generation in all three regimes including squeezing, dripping and jetting modes. (b) Graphical illustration of the variation of droplet diameter with water to oil pressure ratio across all three regimes. (c) The rate of droplet generation as a function of water to oil pressure ratio.

preserve the bond strength. The coating time was optimised to be 3 min from visual inspection and Burst Pressure test as shown in figure 5.

After coating, the COC film is cleaned using acetone and dried with compressed air turning the surface tacky. The solvent treated film was subsequently sandwiched between the plasma treated patterned COC chips and a blank COC wafer at a force of 900 pounds for 4 min in Wabash™ pneumatic press producing the final device. The presence of the blank COC wafer provided robustness to the device and prevented the thin film from cracking under high pressure pumping. The bonded chips showed sufficient bond strength for generating the desired droplets. The schematic of the bonding process is shown in figure 6(a). Microstructure deformation upon bonding was also tested. Microscopic images of the injection molded filter microstructures were taken before and after solvent bonding. As shown in figure 6(b), the structures were not affected by the bonding process making it applicable for desired droplet generation. The optimised solvent bonding process thus facilitated the bonding of hydrophobic COC surface.

## 4. Results and discussion

The fabricated nickel mold was characterized under high resolution microscope. As compared to computer numerical control (CNC) milling, this UV-LIGA technology using SU8 method of mold fabrication produced microfluidic channels with lower feature size (as low as 20 $\mu$m) and steeper side walls. The use of the replaceable mold block further reduces the cost of the produced chips. The fabricated COC chips were solvent cleaned and was coated with a thin film of gold for scanning electron microscopy (SEM). Figure 7 shows the high-resolution features of a single device mold and the SEM images of the features on the final COC chip. This method of mold fabrication combined with optimized solvent bonding technique thus produced reliable and cheap microfluidic droplet generators on thermoplastic.

To characterize the water-in-oil (W/O) droplet generation in the COC device, DI water forms the dispersed phase while HFE 7500 and 1% (w/w) Pico-Surf (Dolomite) constitutes the continuous phase. The fluid injection into the microfluidic chip is realized using a constant pressure source and solenoid valves controlled by customized LabView program (National Instruments). Different regimes of droplet generation were achieved by controlling the relative flow rate of the dispersed and continuous phase. Droplet generation was monitored using Nikon TS 100 microscope and recorded using phantom camera V-310 (Vision Research).

The droplet generation parameters including production rates is measured using ImageJ, a public domain software developed at National Institute of Health. Figure 8 shows the generation of stable, monodisperse water-in-oil droplets in the injection molded COC chip. The orifice diameter is 20 $\mu$m, the oil inlet channels are of 50 $\mu$m width whereas the microfluidic channel carrying DI water has a width of 50 $\mu$m.

Figure 9(a) shows the generation of droplets in squeezing, dripping and jetting regimes in the flow focusing junction geometry. The droplet generation results correlate with the past findings on the chip fabricated using PDMS [37]. The droplet diameter increases linearly with the water to oil pressure ratio in both dripping and squeezing regimes. However, the polydispersity observed in the jetting regimes resulted in a non-linear relationship as shown in figure 9(b). Transition between the three regimes is dictated by the capillary number (Ca). Droplet diameter in squeezing regime is larger than both the dripping and jetting regimes, and it depends on the orifice diameter. Further increase in Ca results in the transition from squeezing to dripping regime. The droplets generated in dripping regime is highly monodisperse (polydispersity $< 2\%$). In the jetting regime, dispersed phase extends like a long jet outside the orifice exit. The droplets generated in this regime have a greater polydispersity. In our experiments, the switching between the regimes is achieved by altering the water phase to oil phase pressure ratio. In both squeezing and dripping regimes, monodisperse droplets are generated at the rate of 70 droplets $s^{-1}$ and 1300 droplets $s^{-1}$ respectively; however, the highest generation rate is achieved in the jetting regimes (2500 droplets $s^{-1}$) as shown in figure 9(c).

The droplet generation rate decreases linearly with increase in the water to oil pressure ratio. This is because of the decrease in the continuous shearing of the oil phase on the water phase at higher water to oil pressure ratios. Also, it is observed that there is an uneven droplet production rate in the jetting regime, and it is due to the hydrodynamic instability jet break-up [47]. Droplet size and the generation frequency within each regime can be changed by precisely controlling the relative flow rates. Larger throughputs can even be achieved but that was not attempted in this study.

## 5. Conclusion

Low cost, mass producible microfluidic droplet generators were successfully fabricated on thermoplastic polymer and stable droplet generation in all three regimes in a flow focusing junction geometry was successfully demonstrated. The results showed the successful development of reliable low-cost injection molded COC polymer chips as a droplet generator. The results obtained are comparable to findings reported on PDMS based droplet generators which ensures the applicability of the fabricated devices. Increasing the contact angle of the natural COC surface and optimising the solvent bonding process to create hydrophobic microfluidic channels for facilitating W/O droplet generation signifies the novelty of this work. The new injection molded and solvent-assisted bonded COC chips developed in this work can pave a new way towards manufacturable high throughput droplet generators for single cell analysis which has the potential to impact a broad range of problems in healthcare, agriculture and environmental monitoring and protection. Such cheap droplet generators can also be used for conducting droplet PCR and thus can aid in the development of point of care diagnostic devices.

## Acknowledgments

The authors would like to acknowledge support from the National Science Foundation and the industrial members of the CADMIM—Center for Advanced Design and Manufacturing of Integrated Microfluidics (NSF I/UCRC award number IIP-1362165).

## ORCID iDs

Sthitodhi Ghosh https://orcid.org/0000-0003-3456-2231

## References

[1] Whitesides G M 2006 *Nature* **442** 368–73
[2] Teh S Y, Lin R, Hung L H and Lee A P 2008 *Lab Chip* **8** 198–220
[3] Squires T M and Quake S R 2005 *Rev. Mod. Phys.* **77** 977–1026
[4] Song H, Chen D L and Ismagilov R F 2006 *Angew. Chem., Int. Ed. Engl.* **45** 7336–56
[5] Macosko E Z *et al* 2015 *Cell* **161** 1202–14
[6] Shembekar N, Chaipan C, Utharala R and Merten C A 2016 *Lab Chip* **16** 1314–31
[7] Agresti J J *et al* 2010 *Proc. Natl Acad. Sci.* **107** 4004–9
[8] Griffiths A D and Tawfik D S 2006 *Trends Biotechnol.* **24** 395–402
[9] Zheng B, Roach L S and Ismagilov R F 2003 *J. Am. Chem. Soc.* **125** 11170–1
[10] Zheng B, Tice J D and Ismagilov R F 2004 *Adv. Mater.* **16** 1365–8
[11] Hammadi Z, Candoni N, Grossier R, Ildefonso M, Morin R and Veesler S 2013 *C. R. Phys.* **14** 192–8
[12] Tan Y-C, Hettiarachchi K, Siu M, Pan Y-R and Lee A P 2006 *J. Am. Chem. Soc.* **128** 5656–8
[13] Li L, Schertzer J W and Chiarot P R 2015 *Lab Chip* **15** 3591–9
[14] Davies R T, Kim D and Park J 2012 *J. Micromech. Microeng.* **22** 055003
[15] Yi G, Thorsen T, Manoharan V N, Hwang M, Jeon S, Pine D J, Quake S R and Yang S 2003 *Adv. Mater.* **15** 1300–4
[16] Lee J and Kim C 2000 *J. Microelectromech. Syst.* **9** 171–80
[17] Zhong Q, Bhattacharya S, Kotsopoulos S, Olson J, Taly V, Griffiths A D, Link D R and Larson J W 2011 *Lab Chip* **11** 2167–74
[18] Hua Z, Rouse J L, Eckhardt A E, Srinivasan V, Pamula V K, Schell W A, Benton J L, Mitchell T G and Pollack M G 2010 *Anal. Chem.* **82** 2310–6
[19] Hatch A C, Fisher J S, Pentoney S L, Yang D L and Lee A P 2011 *Lab Chip* **11** 2509
[20] Schaerli Y, Wootton R C, Robinson T, Stein V, Dunsby C, Neil M A, French P M, Demello A J, Abell C and Hollfelder F 2009 *Anal. Chem.* **81** 302–6
[21] Baker M 2012 *Nat. Methods* **9** 541–4
[22] Holtze C 2013 *J. Phys.: Appl. Phys.* **46** 114008
[23] Hsieh A T H, Pan P J and Lee A P 2014 *Anal. Bioanal. Chem.* **406** 3059–67
[24] Muluneh M, Kim B, Buchsbaum G and Issadore D 2014 *Lab Chip* **14** 4638–46
[25] Romanowsky M B, Abate A R, Rotem A, Holtze C and Weitz D A 2012 *Lab Chip* **12** 802–7
[26] Mukhopadhyay R 2007 *Anal. Chem.* **79** 3248–53
[27] Nisisako T and Torii T 2008 *Lab Chip* **8** 287–93
[28] Tsao C-W 2016 *Micromachines* **7** 225

[29] Chakraborty A, Ghosh S, Han J and Ahn C H 2015 *19th Int. Conf. on Miniaturized Systems for Chemistry and Life Sciences* pp 1271–3
[30] Lee S H, Kim S-W, Kang J Y and Ahn C H 2008 *Lab Chip* **8** 2121–7
[31] Do J, Lee S, Han J, Kai J, Hong C-C, Gao C, Nevin J H, Beaucage G and Ahn C H 2008 *Lab Chip* **8** 2113–20
[32] Keller N *et al* 2016 *Lab Chip* **16** 1561–4
[33] Ahn C H, Choi J-W, Beaucage G, Nevin J H, Lee J-B, Puntambekar A and Lee J Y 2004 *Proc. IEEE* **92** 154–73
[34] Zhou C F, Yue P T and Feng J J 2006 *Phys. Fluids* **18** 092105
[35] Tan Y C, Cristini V and Lee A P 2006 *Sensors Actuators* B **114** 350–6
[36] Woodward A, Cosgrove T, Espidel J, Jenkins P and Shaw N 2007 *Soft Matter* **3** 627–33
[37] Hatch A C *et al* 2011 *Lab Chip* **11** 3838–45
[38] Choi J-W *et al* 2001 *Proc. 5th Int. Conf. MicroTotal Analysis Systems* pp 411–2
[39] Aigars P, Nikcevic I, Lee S H, Ahn C H, Heineman W R, Limbach P A and Seliskar C J 2005 *Lab Chip* **5** 1348–13
[40] Ghosh S, Kurup G K, Lee M S, Lee A P and Ahn C H 2017 *2017 19th Int. Conf. on Solid-State Sensors, Actuators and Microsystems (TRANSDUCERS)* pp 1758–61
[41] Mekaru H, Yamada T, Yan S and Hattori T 2004 *Microsyst. Technol.* **10** 682–8
[42] Kim S, Trichur R, Beaucage G, Ahn C H and Kim B H 2002 *Proc. of the 10th Solid-State Sensor, Actuator and Microsystems Workshop* pp 206–9
[43] Kim K, Park S, Lee J-B, Manohara H, Desta Y, Murphy M and Ahn C H 2002 *Microsyst. Technol.* **9** 5–10
[44] Puntambekar A, Murugesan S, Trichur R, Cho H J, Kim S, Choi J-W, Beaucage G and Ahn C H 2002 *Proc. 6th Int. Conf. Micro Total Analysis Systems* pp 425–7
[45] Ahn C, Kim S, Chao H, Murugesan S and Beaucage G 2002 *Materials Research Society Symp. Proc., BioMEMS and Bionanotechnology*
[46] Hansen C M and Just L 2001 *Ind. Eng. Chem. Res.* **40** 21–5
[47] Christopher G F and Anna S L 2007 *J. Phys.: Appl. Phys.* **40** R319–36